11-17-2020

RF Studies of Soot and Ammonia Loadings on a Combined Particulate Filter and SCR Catalyst

Shreyans Sethia
Michigan Technological University, sssethia@mtu.edu

David Kubinski
Ford Motor Company

Hans Nerlich
Ford Motor Company

Jeffrey Naber
Michigan Technological University, jnaber@mtu.edu

Recommended Citation

Sethia, S., Kubinski, D., Nerlich, H., & Naber, J. (2020). RF Studies of Soot and Ammonia Loadings on a Combined Particulate Filter and SCR Catalyst. *Journal of the Electrochemical Society, 167*(14). http://doi.org/10.1149/1945-7111/abc83e
Retrieved from: https://digitalcommons.mtu.edu/michigantech-p/14416

Follow this and additional works at: https://digitalcommons.mtu.edu/michigantech-p

 Part of the Mechanical Engineering Commons

Journal of the Electrochemical Society

The Electrochemical Society
Advancing solid state & electrochemical science & technology

RF Studies of Soot and Ammonia Loadings on a Combined Particulate Filter and SCR Catalyst

Journal of The Electrochemical Society, 2020 **167** 147516

RF Studies of Soot and Ammonia Loadings on a Combined Particulate Filter and SCR Catalyst

Shreyans Sethia,[1,2] David Kubinski,[2,z] Hans Nerlich,[2,3] and Jeff Naber[1]

[1]*Michigan Technological University, Houghton, Michigan 49931, United States of America*
[2]*Ford Research and Innovation Center, Dearborn, Michigan 48124, United States of America*
[3]*University of Bayrueth, Bayreuth 95440, Germany*

Modern diesels employ a particulate filter (DPF) to reduce soot emissions. Additionally, the selective catalytic reduction (SCR) of NOx by NH_3 stored on the SCR catalyst reduces NOx emissions. In some vehicles the functions of these aftertreatment components are combined in the SDPF, a DPF having a SCR washcoat. The RF resonant method has been shown to be an alternative tool for measuring the DPF's soot loading and the SCR's NH_3 loading. For both applications, the transmitted electromagnetic signal between antennae placed on either side of the catalyst change with loading. Here we report the influence of the RF signal on both soot and NH_3 loadings on a SDPF segment. We show that the attenuation of the RF signal by soot is much larger than that caused by saturating it with 400 ppm NH_3. By taking the mean RF signal amplitude measured over a wide range of frequencies, we demonstrate a method for determination of the soot loading even in the presence of stored NH_3. For "light" soot loadings, before the RF attenuation by soot cause the resonant modes to disappear in the spectra, we demonstrate a method for the simultaneous determination of both the soot and NH_3 loadings.

 [DOI: 10.1149/1945-7111/abc83e]

Manuscript submitted August 11, 2020; revised manuscript received October 27, 2020. Published November 17, 2020. *This paper is part of the JES Focus Issue on IMCS 2020.*

In modern diesel vehicles, the undesired soot emissions are removed via the diesel particulate filter (DPF), a porous ceramic filter typically comprised of SiC, cordierite, or aluminum titanate.[1,2] This filter traps the engine's soot emissions and occasionally requires regeneration to remove the captured soot before it accumulates to a level appreciably impeding the exhaust flow. Regeneration is achieved by raising the exhaust temperature sufficiently to burn the soot trapped on the DPF.[3] Additionally, modern diesel vehicles also have a catalytic exhaust component to reduce their NOx emissions. For this, many diesels use the Selective Catalytic Reduction (SCR) catalyst, which typically has a zeolite washcoat that stores NH_3 introduced into the exhaust via the injection of urea upstream of the SCR.[4–6] The engine out NOx emissions are removed through reactions with the NH_3 stored on the SCR washcoat. The reactive pathways for the NOx reduction by the NH_3 stored on the SCR washcoat are well known.[4,5]

In some diesel vehicles the functions of these two exhaust components are combined in a single catalyst,[7–9] referred to as a SDPF. This is typically a cordierite DPF whose porous walls are coated with the also porous SCR zeolite material. The SDPF serves two functions by trapping the soot and by reducing the NOx emissions. As with the SCR, the latter is accomplished via reactions with NH_3 stored on the SCR zeolite washcoat. Like the DPF, the SDPF must be occasionally regenerated to burn off the accumulated soot. For both these soot filters, the high temperature regeneration is triggered via the use of a differential pressure sensor. As the captured soot builds to a maximum desired loading, a threshold pressure differential across the filter is reached triggering a thermal regeneration.[10]

As an alternative to the differential pressure sensor, the radio frequency (RF) measurement technique has been shown to be a viable method for measurement of the amount of soot loaded onto DPF's.[11–19] This technique has been shown to offer greater sensitivity, especially at lower exhaust flow rates.[15] Additionally, other studies have demonstrated the technique's utility in determining the amount of NH_3 stored on SCR catalysts.[20–28] In one configuration of the RF method, a microwave resonant cavity is formed by the cylindrical metal can encasing the catalyst. Two metal probes acting as antennas are placed on either side of the catalyst, each located between the catalyst face and a porous metallic screen defining the end face of the cylindrical metal cavity. Power transmitted between the antennae is both generated and detected by a Network Analyzer as the frequency of the signal is swept. At certain frequencies, determined by the cavity's geometry and the dielectric properties and size of the catalyst, electromagnetic resonance is achieved. Measurements of the resonance frequencies, the signal amplitude at resonance, the quality factor at resonance, and the RF amplitude averaged over a frequency range all give information on the dielectric properties of the catalyst.[11,29] For the DPF and the SCR catalysts, these properties change with the soot and NH_3 loading, respectively.[11] The changes in these parameters can be calibrated enabling the use of the RF method as a tool to measure either the soot loading on the DPF or NH_3 loading on the SCR.

In this work we combine the RF studies of soot on the DPF and NH_3 on the SCR and show how the RF signal transmitted to the downstream antenna from that generated upstream is influenced by both the soot and NH_3 loadings on the SDPF. This study is similar to that reported elsewhere for a SDPF core.[30] In our study we show a method for how the soot loading can be determined with little influence by the stored NH_3. We also demonstrate for the case of "light" soot loading, before the attenuation of the signal by the soot dominates the RF response, an alternative method for the simultaneous determination of both the soot and NH_3 loadings on the SDPF.

Experimental

The SDPF used in our measurement was 4.4 cm diameter by 17.4 cm in length, cored from a larger piece used in serial application. It was mounted tightly near the center of a stainless-steel tube with an inner diameter of about 4.8 cm. Shown in Fig. 1, a microwave resonance cavity was formed by placing stainless-steel screens 31 cm apart with the SDPF located in the center. An antenna was positioned between each face of the SDPF and the stainless screen defining the cavity's end face. The antennae were 2 mm DIA stainless-steel rods, aligned perpendicular to the axis of the cavity but parallel to each other. Each penetrated about halfway to the central axis of the tube. Both antennae were connected to an Agilent E5071C network analyzer and the magnitude of the S_{21} transmission parameter, $|S_{21}|$, was measured as a function of frequency. The S_{21} scattering parameter is the power detected at the downstream antenna (denoted as "2") relative to the power radiated into the cavity by the upstream antennae (denoted as "1"). For our studies,

[z]E-mail: dkubinsk@ford.com

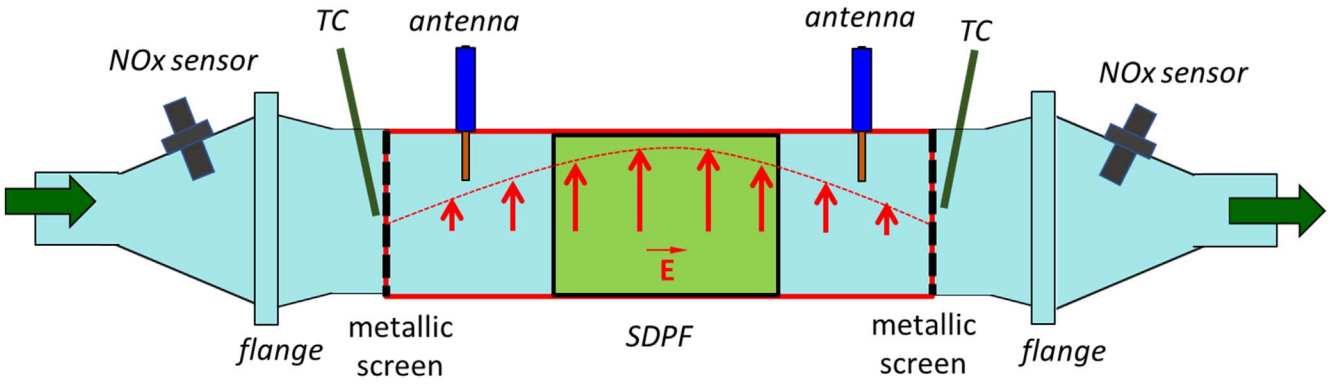

Figure 1. Schematic of the cylindrical resonant cavity and SDPF placed within. Shown are the screens, NOx sensors, thermocouples (TC) and flanges. Overlaid is a plot of the electric field variation along the cavity axis for the fundamental resonant mode.

we report the variation in amplitude (in dB) of the measured $|S_{21}|$ response scanned over a range of frequencies. We also report the mean $|S_{21}|$ amplitude (in dB) determined via integration over both wide and narrow frequency ranges, plus the frequency and amplitude of a particular S_{21} resonant peak. These parameters are similar to those presented in other RF studies.[11,18,29]

A humidified gas flow of 60 l min^{-1} was used in our experiments with water concentration fixed at 2% molar. Temperature of the SDPF was varied using an in-line heater located upstream the portion shown in Fig. 1. The SDPF temperatures we report are the mean of upstream and downstream thermocouples which were each placed a few mm away from the center of the stainless-steel screens but outside the resonant cavity. The portion of the resonant cavity containing the SDPF was not heated externally. This contributed to the observed temperature drop across the length of the cavity and most likely resulted in the temperature decreasing in a radial direction as well. However, at our steady-state measurement points we expect that the temperature profile of the SDPF was unchanging, and we do not believe a lack of an external heater influenced the overall conclusions of this paper. The composition of the outlet gas was monitored with a FTIR analyzer (MIDAC) placed downstream of the cavity. Additionally, automotive NOx sensors, which are used in serial application on diesel vehicles and which are also sensitive to NH_3 as they oxidize it to NO in its first internal chamber, were placed both upstream and downstream of the cavity.

Before RF measurements were done, the SDPF, empty of both soot and NH_3, was loaded at room temperature with soot generated by a benchtop Jing miniCAST 5201C via a controlled propane diffusion flame. A more detailed description of the soot generator and the setup used to load the filter is given elsewhere.[31–33] As depicted in Fig. 2, the portion of the setup between the flanges shown in Fig. 1 was removed and placed on a different flow bench for this purpose. The antennae were removed for the soot loading procedure and in their locations a differential pressure sensor was placed to monitor the pressure drop across the SDPF as it was loaded with soot. The differential pressure sensor was not calibrated for our application and was used just as an additional verification of continual capture of soot by the SDPF. The mean mobility diameter of the soot generated by the setting used for the miniCAST was previously measured to be approximately 100 nm using a Scanning Mobility Particle Sizer. It has also been shown that the black carbon (BC) fraction of this soot is nearly 100%.[32] The size of the miniCAST soot used was larger than the roughly 70 nm particles typical of diesel exhaust, as was the BC fraction which for diesels is typically ~80%–100%.[32] The output of the soot generator was diluted with N_2, and a flow of 90 l min^{-1} was used for loading. The soot concentration during the loadings was measured occasionally by an AVL Micro Soot Sensor and was near 10 mg m^{-3}. This value varied slightly for each of the targeted loadings. The mass of soot loaded onto the SDPF was determined by the product of the mean soot concentration measured by the Micro Soot Sensor and the total flow monitored occasionally with a digital flowmeter positioned downstream. As shown in Table I, eight different soot loading values were used including the empty case, with the maximum 1.37 grams corresponding to a soot density of 5.18 g l^{-1} the SDPF. This value is slightly less than the maximum expected in application. We estimate our measurement of the mass of soot loaded onto the SDPF has an accuracy of ±10%. The same SDPF and fixture as shown in Fig. 2 was used for all the loading cases.

After each instance that the SDPF was loaded with soot, the antennae were re-attached, and the segment between the flanges shown in Fig. 1 was placed back onto our heated gas flow system for the RF measurements. The RF response was measured as a function of temperature, and later at ~230 °C after saturating the SDPF with an input stream of 400 ppm NH_3. All RF measurements reported here were made in background concentrations of 5% O_2 and 2% water. For each of the soot loadings, the typical RF experiment on the sooted SDPF consisted of the following steps:

1. First, we characterized the temperature dependence of the RF response of the sooted SDPF by stepwise measurements at five

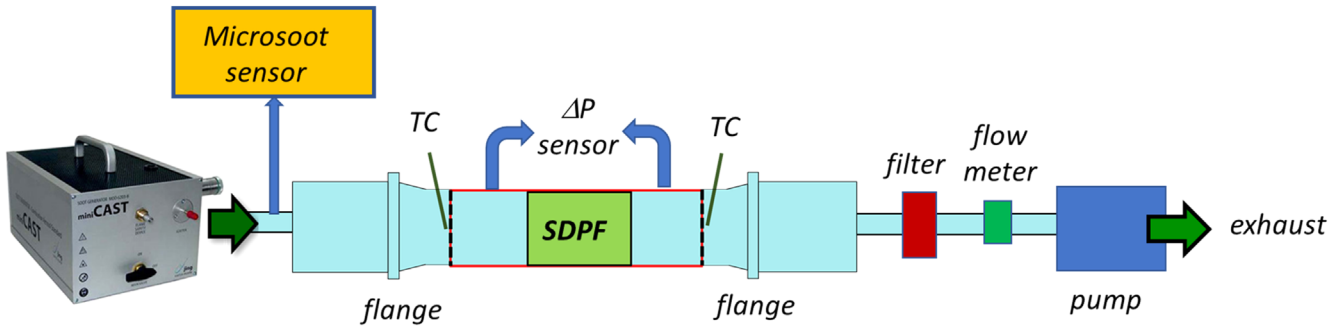

Figure 2. Schematic of the soot loading set-up.

Table I. The eight cases of soot loading on the SDPF used in our studies.

Grams of soot loaded onto SDPF	Soot loading density (grams per volume SDPF)	Time required to load soot
0 g	0 g l^{-1}	0 h
0.05 g	0.19 g l^{-1}	0.83 h
0.14 g	0.53 g l^{-1}	2.5 h
0.18 g	0.68 g l^{-1}	3.0 h
0.41 g	1.55 g l^{-1}	6.83 h
0.73 g	2.76 g l^{-1}	12.0 h
0.76 g	2.87 g l^{-1}	12.33 h
1.37 g	5.18 g l^{-1}	24.0 h

different temperature levels between ~90 °C and ~500 °C. The SDPF temperature profile was held nearly constant typically for more than five minutes at each of these steps, and the RF values we report are those at the end of each step. These stepwise temperature values varied between the eight loading tests, but all were below the temperature at which we expect the soot to oxidize or components to volatize, especially considering that for the CAST setting used the soot was essentially all black carbon.[32]

2. The SDPF temperature was then stabilized at ~230 °C. After that, a constant stream of 400 ppm NH_3 was introduced and kept on until the readings of the downstream NOx sensor (sensitive to NH_3) and the downstream FTIR NH_3 both reached a nearly steady-state level. This way we obtained both the RF response of the sooted SDPF at ~230 °C when it was empty of NH_3 and after it was saturated by the 400 ppm NH_3 input. This was done for all but the 2.76 g l^{-1} soot loading case.
3. After the NH_3 response was measured, the SDPF temperature was raised to ~620 °C while the accompanying O_2 concentration was increased to 16%. During this time the NH_3 desorbed and the soot on the SDPF was oxidized. The temperature was held at ~620 °C for typically one hour until the RF amplitude of the fundamental resonant mode was the same as it was for the case of the empty SDPF.
4. The O_2 was returned to 5% and the SDPF was stepped down in temperature to ~100 °C in five steps to obtain the temperature dependence of the RF response of the empty SDPF. A comparison of the results to the data obtained for the empty soot case verified removal of all the soot and NH_3.

Results

Soot loading in the absence of NH_3 storage on the SDPF.— Figure 3 shows the RF $|S_{21}|$ amplitude spectra (measured in dB) over the frequency range 2.7 GHz–4.7 GHz. Shown are the spectra for the eight different soot loading levels, including the empty case, all measured at a mean SDPF temperature of ~230 °C and with it empty of NH_3. Multiple resonant peaks are seen for the case of 0 g l^{-1} soot loading. The first four peaks in order of frequency are the TE_{111}, TE_{112}, TE_{113} and the TE_{114} resonant modes. The TE_{111} is the fundamental resonant mode. The electric field of the higher frequency TE_{11n} modes have the same radial and angular profile as the fundamental, but instead have n half-wavelengths along the axial direction of the cavity. Upon increasing the soot loading, the amplitude of the resonant peaks become diminished and shifted to slightly lower frequencies. Additionally, the mean value of the entire spectra became reduced as the soot attenuates the transmitted signal. All evidence of the resonant peaks disappears for soot loadings of 1.55 g l^{-1} and greater.

The variation in the $|S_{21}|$ spectra with SDPF temperature in the range ~90 °C to ~500 °C is shown in Figs. 4a–4d. Shown are data for the soot loading cases of 0 g l^{-1}, 0.68 g l^{-1}, 2.76 g l^{-1} and 5.18 g l^{-1}. As seen most clearly for the largest soot loading case shown in Fig. 4d, the $|S_{21}|$ amplitude decreases with increasing temperature, the result of the soot causing more attenuation as the temperature increases. The decrease in RF amplitude with increasing temperature is less for the lower soot loading cases. Figure 5 plots the mean RF amplitude, averaged over the range 2.8 GHz to 4.66 GHz, as a function of the mean SDPF temperature. Shown are data for all eight soot loading cases. This plot demonstrates that the mean RF amplitude decreases as more soot is loaded, and that the variation in the spectra with SDPF temperature is greater for the higher soot loading cases. These results are a consequence of the soot becoming more electrically conductive with increasing temperature, thus more attenuating to the RF signal. The variation in the $|S_{21}|$ spectra with soot loading shown in Fig. 3 and the corresponding temperature dependence of the mean value of $|S_{21}|$ over a fixed frequency range shown in Fig. 5 are qualitatively similar to published results for the measurement of soot loading on an aluminum titanate DPF.[18] Figure 6 gives the mean RF amplitude, averaged between the range 2.8 GHz to 4.66 GHz, as a function of soot loading. Shown are data for mean SDPF temperatures of 200 °C, 300 °C and 400 °C which have been obtained by linearly interpolating data from the previous figure. The error bars represent the ±10% uncertainty in the estimation of the loaded soot mass. Figure 6 demonstrates an approximately linear decrease in the mean RF amplitude with soot loading, with a larger magnitude of slope for the higher temperature. The data points for the three temperatures are all nearly the same for the case of 0 g l^{-1} soot loading, as for that case there is little variation in the mean RF amplitude with SDPF temperature over the frequency range chosen. Ignoring any potential influence due to stored NH_3, the data shown in Figs. 5 and 6 can be used as a calibration for the determination of the amount of soot loading on SDPF.

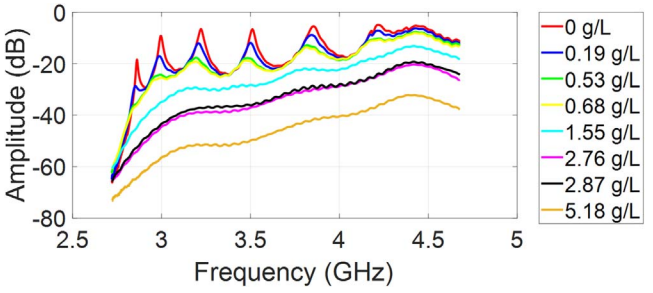

Figure 3. The RF $|S_{21}|$ amplitude spectra over the frequency range 2.7–4.7 GHz for the eight different soot loading levels. All measured at a mean SDPF temperature of ~230 °C and with it empty of NH_3.

Soot loading in the presence of NH_3 storage on the SDPF.— After the temperature dependency of the RF response was measured for each soot loading case, the SDPF mean temperature was stabilized at ~230 °C and 400 ppm NH_3 was introduced and kept on until the SDPF became saturated by it. This was indicated by nearly constant high readings of NH_3 downstream of the SDPF by both the FTIR and by the NOx sensor (which is sensitive to NH_3). We estimate the mean density of NH_3 stored on the SDPF to have been about 1.7 ± 0.2 g l^{-1} which was determined from the integrated differences in the NH_3 gas concentrations upstream and downstream of the SDPF, a technique reported elsewhere.[20] This value did not appear to be effected by the accompanying levels of soot also stored on the SDPF. Figures 7a–7c

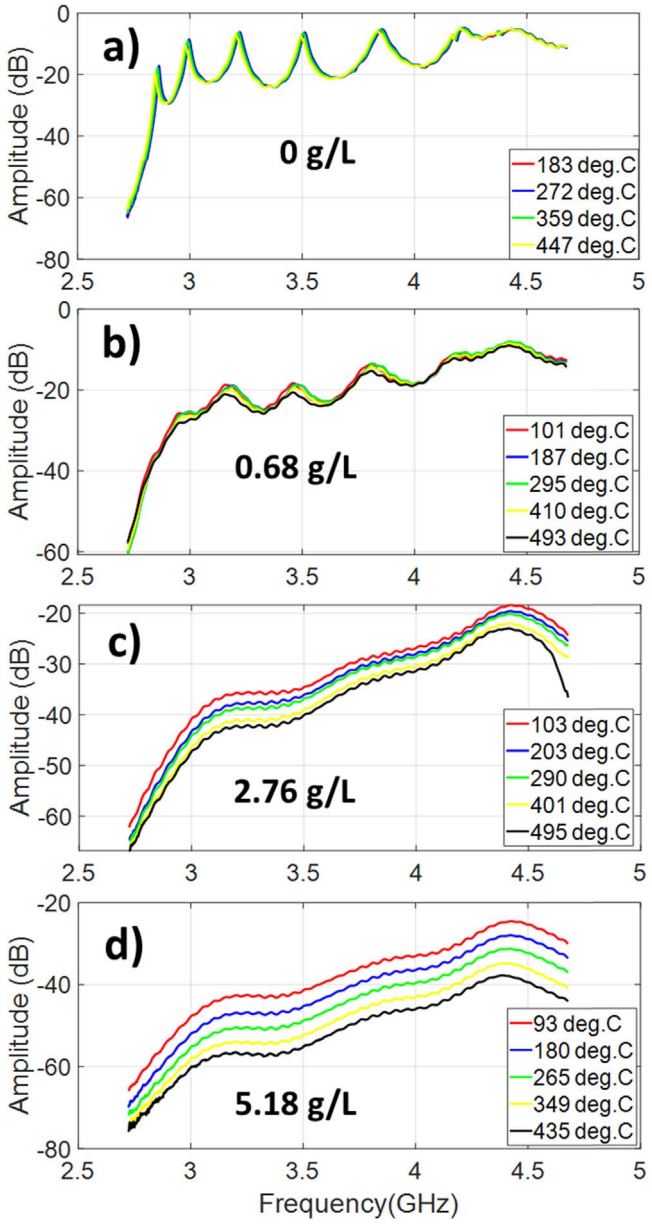

Figure 4. The RF $|S_{21}|$ amplitude spectra measured at different mean SDPF temperatures. Shown in (a)–(d) are data for the cases of 0 g l^{-1}, 0.68 g l^{-1}, 2.76 g l^{-1} and 5.18 g l^{-1} soot loading levels, respectively. All were measured with the SDPF empty of NH_3.

compares the $|S_{21}|$ RF spectra at ~230 °C just before the NH_3 was introduced with that taken after the SDPF was saturated by the 400 ppm NH_3. Shown are the results for 0 g l^{-1} soot loading in Fig. 7a, 0.53 g l^{-1} in Fig. 7b, and 1.55 g l^{-1} in Fig. 7c. Comparing the two spectra for the case of 0 g l^{-1} soot loading, saturating the SDPF with the NH_3 reduces the amplitudes of the first four resonant peaks by about ~5 dB to ~3 dB, with the amount of attenuation differing for each peak. The resonant peaks are also shifted to slightly lower frequencies. These trends are consistent with that reported elsewhere for RF measurements of the NH_3 loading on SCR catalysts, and careful analysis of these data can be used to quantify the NH_3 loading on the soot-free SCR.[21,23,26] Comparing the NH_3-free cases in Figs. 7a and 7b, we see that 0.53 g l^{-1} soot loading on the SDPF attenuates the first four resonant peaks by about ~16 dB to ~10 dB, much more than the attenuation caused by the 400 ppm NH_3 saturation of the soot-free SDPF seen in Fig. 7a. For the 0.53 g l^{-1} soot loading case, the resonant peaks were only attenuated ~1 dB to ~2 dB further after

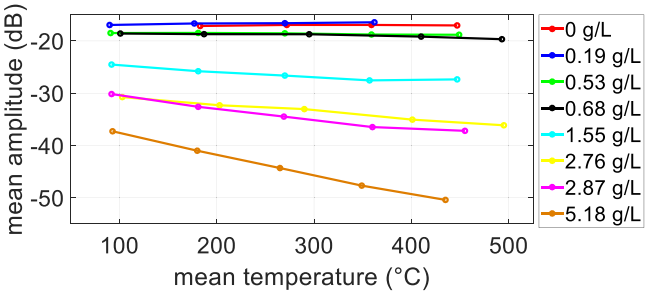

Figure 5. The mean RF $|S_{21}|$ amplitude, averaged over the frequency range 2.8 GHz–4.66 GHz, plotted as a function of the mean SDPF temperature. Shown are data for all eight soot loading levels and are all for the case of the SDPF empty of NH_3.

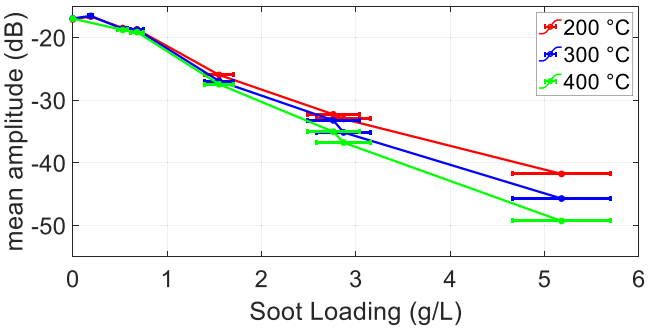

Figure 6. The mean RF $|S_{21}|$ amplitude, averaged over the frequency range 2.8 GHz–4.66 GHz, plotted as a function of soot loading. Shown are data for mean SDPF temperatures of 200 °C, 300 °C and 400 °C.

saturating the SDPF with the NH_3, a smaller influence on the amplitude than the same NH_3 addition had on the soot-free SDPF. However, the 400 ppm NH_3 saturation on the 0.53 g l^{-1} soot-loaded SDPF still shifted the resonant peaks to lower frequencies. The higher soot loading case of 1.55 g l^{-1} shown in Fig. 7c demonstrates further attenuation of the RF signal by the soot. For this case the resonant peaks are no longer evident and saturating the SDPF with 400 ppm NH_3 had little effect on the RF response.

Figure 8a plots the mean RF amplitude at ~230 °C, averaged over the frequency range from 2.8 GHz to 4.66 GHz, as a function of soot loading. Shown are the data for the cases of the SDPF empty of NH_3 and after it was saturated by the 400 ppm NH_3 input. Both curves are nearly identical, showing an approximate linear decrease with soot loading. This plot demonstrates that it is possible to determine the amount of soot loading on the SDPF independent of the NH_3 loading. For the soot loading cases of 0.68 g l^{-1} and less, which we refer to a "light" soot loading and which represents less than ~10% of the typical maximum loading, we observed that after saturation by 400 ppm NH_3 the resonant peaks were shifted to slightly lower frequencies and became diminished in amplitude (more so with less soot loading). However, the mean of the spectra over this wide frequency range encompassing many resonant modes was not much affected by the ammonia storage. Figure 8b plots again the mean RF amplitude vs the soot loading, but in this figure the RF amplitude was averaged over 4.36 GHz to 4.66 GHz, a narrower frequency range and one away from the sharp resonant peaks. These data also show a nearly linear decrease in the mean amplitude with soot loading with little influence due to saturation by the 400 ppm NH_3, demonstrating the frequency range used to obtain the results of Fig. 8a was not unique.

Discussion

Closer examination of the data for the "light" soot loading cases, where the resonant modes are still visible, reveals the possibility of

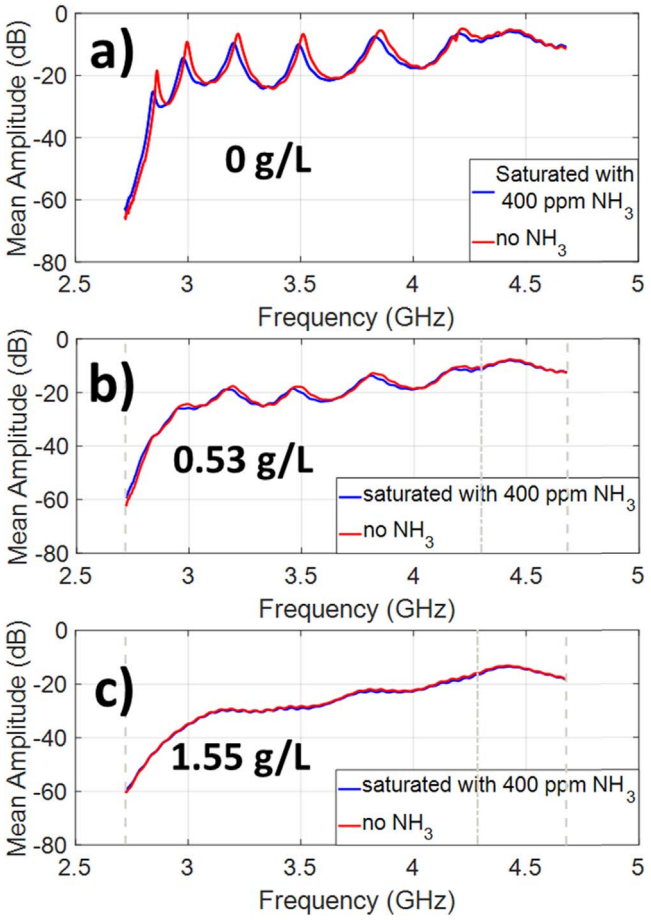

Figure 7. The RF $|S_{21}|$ amplitude spectra at ∼230 °C measured with it empty of NH_3 (red) and after saturating the SDPF with a 400 ppm NH_3 input stream (blue). Shown in (a)–(c) are data for soot loading levels of 0 g l^{-1}, 0.53 g l^{-1} and 1.55 g l^{-1}, respectively.

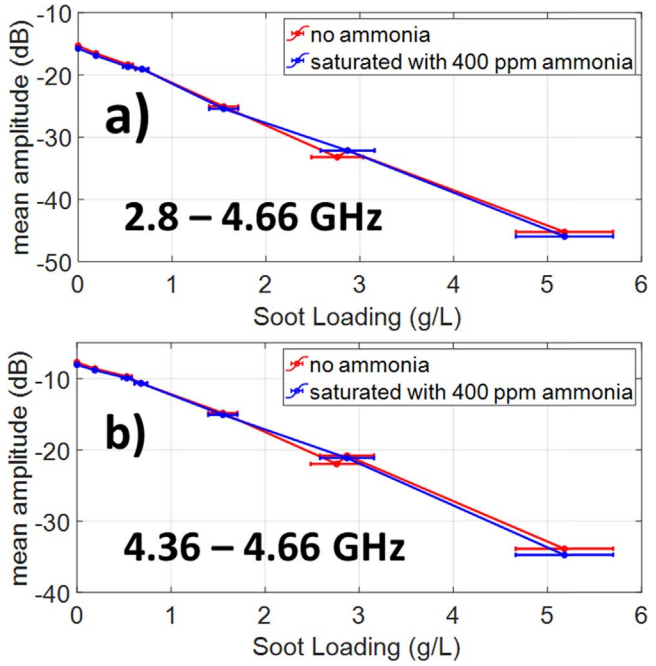

Figure 8. The mean RF $|S_{21}|$ amplitude at ∼230 °C plotted as a function of the SDPF's soot loading level. Shown are data for the cases of the SDPF empty of NH_3 (red) and after saturating it with a 400 ppm NH_3 input stream (blue). Shown in (a) are data for the RF amplitude averaged over the range 2.8 GHz–4.66 GHz, and in (b) the narrower range of 4.36 GHz–4.66 GHz. These two frequency ranges are indicated by the vertical dashed grey lines in Figs. 7b and 7c.

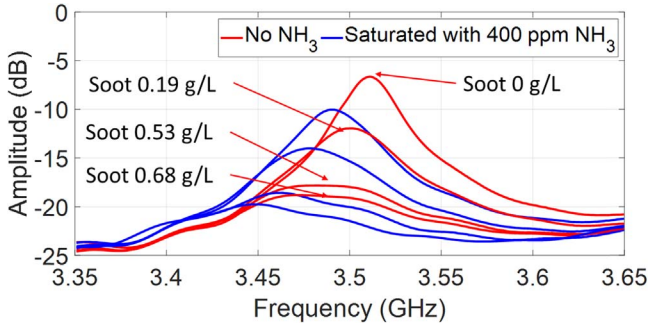

Figure 9. The RF $|S_{21}|$ amplitude spectra at ∼230 °C for the fourth resonant peak. Shown are data for the four lowest soot loading cases, 0 g l^{-1}, 0.19 g l^{-1}, 0.53 g l^{-1} and 0.68 g l^{-1}. The data plotted in red are for the case of the SDPF empty of NH_3, and in blue after saturating it with a 400 ppm NH_3 input stream. The heights of the peak amplitudes for the NH_3 loading case in blue are in the same order as for the case of no NH_3 shown in red.

simultaneous measurement of both the soot and NH_3 loading via the RF method. Figure 9 shows in a magnified view the influences of both soot and NH_3 loading for one of the resonant peaks, the TE_{114}, taken at ∼230 °C. Data for the other resonant peaks are qualitatively similar. Shown in the figure are the four cases of "light" soot loading, up to 0.68 g l^{-1} and which only represents up to 13% of the soot loading range we investigated. As previously discussed, both the measured resonance frequency and the signal amplitude at resonance are observed to decrease with soot loading, and again after NH_3 saturation by the 400 ppm loading. These trends are qualitatively similar to results for the fundamental resonant mode reported elsewhere for measurement on a cordierite-based SDPF.[30] The influence of the soot loading on the RF amplitude at resonance for the mode in Fig. 9 is plotted in Fig. 10a for the cases of with and without NH_3 loading. The corresponding influence of the resonant frequency is shown in Fig. 10b. In Fig. 10 we used the real and imaginary components of the complex S_{21} amplitude spectra to determine both the resonant frequency and amplitude at resonance, following the same method as reported elsewhere.[29] Note that the difference in the resonant frequency seen in Fig. 10b for the data corresponding to the cases with and without NH_3 loading is about ∼0.02 GHz for all the four "light" soot loading cases. A similar constant separation in the curves is not observed for the corresponding amplitude data shown in Fig. 10a.

We demonstrate that by using the curves in Figs. 10a and 10b, simultaneous estimation of both the soot and NH_3 can be accomplished for these "light" soot loading cases. For example, an amplitude measurement −12 dB as seen in Fig. 10a indicates the soot loading can be either ∼0.09 g l^{-1} or ∼0.19 g l^{-1}, dependent upon whether or not it was loaded by the 400 ppm NH_3 input stream. However, these two possibilities can be distinguished from each other by the value of the corresponding resonant frequency. Additionally, either of the curves of Fig. 10 can be used to distinguish between the two NH_3 loading cases if the soot loading was determined using the mean amplitude method shown in Figs. 8a or 8b.

We recognize that the saturation storage level of NH_3 on a SCR washcoat catalyst is dependent on both the input NH_3 concentration and the catalyst temperature, as is the corresponding RF response.[20,21,26] Our study of the NH_3 loading on the SDPF only investigated a single concentration and temperature. As the attenuation of the RF response is dominated by the soot, we still expect the methods demonstrated here are viable approaches. Further studies would verify the robustness of the results of Figs. 8 and 9 to other

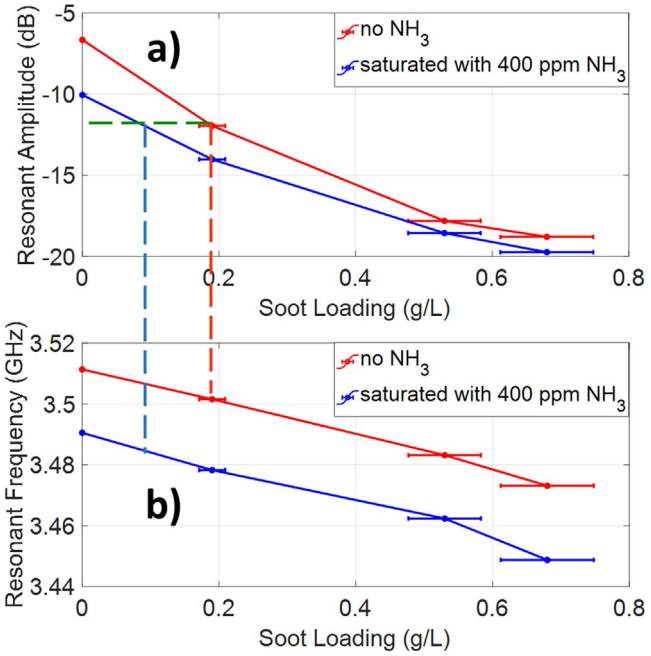

Figure 10. In Fig. 10a the amplitude at resonance determined from the data in Fig. 9 is plotted against the soot loading. Figure 10b plots the corresponding resonant frequency. Shown in both figures are data for the SDPF empty of NH_3 (red) and after saturating it with a 400 ppm NH_3 input stream (blue). The vertical dashed lines indicated how values with the same amplitude at resonance can have different resonant frequencies dependent upon the NH_3 loading.

NH_3 levels and temperatures. A calibration of the variation in both resonant frequency and the corresponding amplitude at resonance as a function of NH_3 loading can be made for each incremental soot loading case. Additionally, this would have to be done as a function of SDPF temperature. Although this would entail a substantial calibration effort, it is at least possible. However, the important point is that in our approach the simultaneous determination of both soot and NH_3 loadings is only possible for cases of "light" soot loading, when the resonance peaks can still be observed. The resonance peaks disappear for the cases of $1.55\,g\,l^{-1}$ of soot loading and greater as the attenuation by soot dominates the $|S_{21}|$ signal. The spectra for those cases show little influence on the NH_3 loading, and for these the NH_3 loading cannot be determined in our approach. Our method for simultaneous determination of both soot and NH_3 loadings differs from that previously reported[30] in that we could only determine NH_3 loadings for the "light" soot loading cases. However, we demonstrate that for all cases the soot loading can still be determined using the frequency averaged $|S_{21}|$ curves from Figs. 8a and 8b. Noise factors, such as ash loading were not part of this study. Additional studies would be required to characterize it's influence on the simultaneous measurement of soot and NH_3 on the SDPF.

Conclusions

In summary, this report demonstrates that the attenuation of the $|S_{21}|$ RF signal by soot far outweighs that caused by the NH_3 storage from the 400 ppm input stream. We show a method for the determination of the soot loading on a SDPF independent of its NH_3 loading by integrating the RF spectra over a wide range of frequencies encompassing many resonant modes which are visible for the low soot loading cases, or over by integration over a narrower frequency range away from the resonant modes. We also demonstrate that for the cases of "light" soot loading, where the attenuation of soot is not so great as to eliminate the resonant peaks, simultaneous determination of both the soot and NH_3 loading is possible.

Acknowledgments

The authors would like to acknowledge Dr. Xin Lu of the Ford Research and Innovation Center for her assistance setting up the soot loading of the SDPF. We would also like to acknowledge Garlan Huberts, also from Ford, for arranging for the internship of Shreyans Sethia and Prof. Ralf Moos, U. Bayreuth, for arranging the internship of Hans Nerlich.

ORCID

David Kubinski https://orcid.org/0000-0001-5821-8756

References

1. T. Boger, J. Jamison, J. Warkins, N. Golomb, C. Warren, and A. Heibel, *SAE 2011 World Congress and Exhibition* (2011), *SAE Technical paper*, 2011-01-0816.
2. W. Cutler, T. Boger, A. Chiffey, P. Phillips, D. Swallow, and M. V. Twigg, *SAE World Congress and Exhibition* (2007), *SAE Technical paper*, 2007-01-1268.
3. M. Nakamura and M. Ozawa, *2019 JSAE/SAE Powertrains, Fuels and Lubricants Meeting* (2019), *SAE Technical paper*, 2019-01-2288.
4. G. Cavataio, H. Jen, J. Warner, J. Girard, J. Kim, and C. Lambert, *SAE Int. J. Fuels Lubr.*, **1**, 477 (2009).
5. G. Cavataio, J. Girard, and C. Lambert, *SAE World Congress and Exhibition* (2009), *SAE Technical paper*, 2009-01-0897.
6. G. Guo, D. Dobson, J. Warner, W. Ruona, and C. Lambert, *SAE 2012 World Congress and Exhibition* (2012), *SAE Technical paper*, 2012-01-0371.
7. J. Tan, C. Solbrig, and S. Schmieg, *SAE 2011 World Congress and Exhibition* (2011), *SAE Technical paper*, 2011-01-1140.
8. M. Naseri, S. Chatterjee, M. Castagnola, H.-Y. Chen, J. Fedeyko, H. Hess H., and J. Li, *SAE 2011 World Congress and Exhibition* (2011), *SAE Technical paper*, 2011-01-1312.
9. Y. Jin, N. Shinoda, Y. Uesaka, T. Kuki, M. Yamashita, H. Sakamoto, T. Matsumoto, P. Kattouah, and C. Dieter Vogt, *JSAE/SAE 2015 International Powertrains, Fuels and Lubricants Meeting* (2015), *SAE Technical paper*, 2015-01-2018.
10. E. Xuereb and M. Farrugia, *SAE 2016 International Powertrains, Fuels and Lubricants Meeting* (2016), *SAE Technical paper*, 2016-01-2280.
11. R. Moos, *SAE Int. J. Engines*, **8**, 1240 (2015).
12. A. Sappok and L. Bromberg, *SAE Int. J. Commer. Veh.*, **7**, 466 (2014).
13. A. Sappok, L. Bromberg, J. Parks, and V. Prikhodko, *SAE 2010 Powertrains Fuels and Lubricants Meeting* (2010), *SAE Technical paper*, 2010-01-2126.
14. A. Sappok, P. Ragaller, L. Bromberg, V. Prikhodko, J. Storey, and J. Parks, *SAE 2016 World Congress and Exhibition* (2016), *SAE Technical paper*, 2016-01-0918.
15. P. Ragaller, A. Sappok, L. Bromberg, N. Gunasekaran, J. Warkins, and R. Wilhelm, *SAE 2016 World Congress and Exhibition* (2016), *SAE Technical paper*, 2016-01-0943.
16. A. Sappok, P. Ragaller, A. Herman, L. Bromberg, V. Prikhodko, J. Parks, and J. Storey, *SAE Int. J. Engines*, **10**, 1667 (2017).
17. A. Sappok, P. Ragaller, A. Herman, L. Bromberg, V. Prikhodko, J. Parks, and J. Storey, *WCX World Congress Experience* (2018), *SAE Technical paper*, 2018-01-1260.
18. M. Fuelner, F. Seufert, A. Müller, G. Hagen, and R. Moss, *Top. Catal.*, **60**, 374 (2017).
19. S. Walter, P. Schwanzer, G. Hagen, G. Haft, H.-P. Rabl, M. Dietrich, and R. Moos, *Sensors*, **20**, 2659 (2020).
20. D. Rauch, D. Kubinski, G. Cavataio, D. Upadhyay, and R. Moos, *SAE Int. J. Engines*, **8**, 1126 (2015).
21. D. Rauch, D. Kubinski, U. Simon, and R. Moos, *Sens. Actuators B: Chem.*, **205**, 88 (2014).
22. D. Rauch, G. Albrecht, D. Kubinski, and R. Moos, *Appl. Catal. B: Env.*, **165**, 36 (2015).
23. M. Dietrich, C. Steiner, G. Hagen, and R. Moos, *SAE Int. J. Engines*, **10**, 1638 (2017).
24. M. Dietrich, D. Rauch, A. Porch, and R. Moos, *Sensors*, **14**, 16856 (2014).
25. D. Kubinski and A. Bogner, *Procedia Engineering*, **168**, 11 (2016).
26. M. Dietrich, G. Hagen, W. Reitmeier, K. Burger, M. Hien, P. Grass, D. Kubinski, J. Visser, and R. Moos, *Sensors*, **17**, 1615 (2017).
27. M. Dietrich, G. Hagen, W. Reitmeier, K. Burger, M. Hien, P. Grass, D. Kubinski, J. Visser, and R. Moos, *Sensors*, **17**, 2746 (2017).
28. P. Ragaller, J. Mandelbaum, L. Lapenta, A. Sappok, J. Pihl, V. Prikhodko, and J. Parks II, *Proceedings of the ASME 2019 Internal Combustion Engine Division Fall Technical Conference, ICEF2019-7224* (2019).
29. M. Dietrich, C. Jahn, P. Lanzerath, and R. Moos, *Sensors*, **15**, 21971 (2015).
30. P. Ragaller, A. Sappok, J. Qiao, X. Liu, and J. Aguilar, *Proceedings of the ASME 2018 Internal Combustion Engine Division Fall Technical Conference, ICEF2018-9528* (2018).
31. R. Moore, L. Ziemba, D. Dutcher, A. Beyersdorf, K. Chan, S. Crumeyrolle, T. Raymond, K. Thornhill, E. Winstead, and B. Anderson, *Aerosol Sci. Technol.*, **48**, 467 (2014).
32. M. Maricq, *Aerosol Sci. Technol.*, **48**, 620 (2014).
33. X. Liu, T. Chanko, C. Lambert, and M. Maricq, *WCX World Congress Experience* (2018), *SAE Technical paper*, 2018-01-1259.